Effects of Soil-Structure Interaction on Wall Deflections and Surface Settlements During Deep Excavations

L.W. Wong

SMEC Asia Limited, Hong Kong

doi: https://doi.org/10.21467/proceedings.159.7

ABSTRACT

Ground movements due to excavations may cause damages to structures. While wall deflections could be adequately predicted, accurate estimations of ground movements are usually far from field observations. It has been identified that the behaviour of soil at small strain plays a key role in predicting the surface settlements. Presented herein is a study on a well-documented excavation case history in soft ground located in Taipei Basin. Two-dimensional finite element analyses adopting the hardening soil with small-strain stiffness to simulate the nonlinear stress-strain relationship of soils have been conducted. Various interface reduction factors have been adopted to simulate the soil-structure interaction. The effect of water pressures on the performance of excavations was studied. The analyzed results show that the hardening soil with small-strain stiffness model could reliably predict the wall deflections and the surface settlements simultaneously. The interface reduction factor would be the key parameter for exploring the ground movements due to deep excavations.

Keywords: Soil-structure Interaction, Hardening-Soil Model, Small Strain, Ground Movements

1 Introduction

The prediction by numerical analysis on surface settlements next to excavations has been the challenge of the researchers and the practicing profession. Jardine *et al.* (1986) and Burland (1989) pointed out that as soil displays non-linear behavior and the stiffness of soils at small strain is very high, the small-strain behaviour of soil plays an important role on predicting the ground surface settlements induced by excavation.

In order to investigate the importance of the nonlinear behavior of soil on predicting the ground surface settlements, Kung *et al.* (2009) conducted numerical analysis on a case history using various soil models. Amongst the models adopted in the analysis, they found that good predictions on surface settlements could be obtained by using the Modified Pseudo-Plasticity model (Kung, 2003) and by the Three-Surface Kinematic Hardening model (Stallebrass & Taylor, 1997). These 2 soil models consider high initial stiffness of soil and nonlinear behavior at small strain. The other soil models, the Modified Cam-clay model (Roscoe &. Burland, 1968) and the Original Hyperbolic model Duncan & Chang (1970), Kondner & Zelasko (1963), cannot properly predict the surface settlements. Kung & Ou (2006) confirmed the importance of behavior of soil at small strain on the prediction of excavation behaviour.

The Modified Pseudo-Plasticity model and the Three-Surface Kinematic Hardening model are in-house programs of the research or the academic institutes and are not readily available by the practicing professionals. On the other hand, the Hardening-Soil with small-strain Stiffness model (HSS) developed by Benz Thomas (2006) and introduced in the PLAXIS program (PLAXIS 2013) is commercially available. Since the HSS model simulates the nonlinear stress-strain-strength relationship of soils, it is expected that the HSS model could be applicable for predicting the behavior of surface settlements induced by excavations.

Proceedings DOI: 10.21467/proceedings.159; Series: AIJR Proceedings; ISSN: 2582-3922; ISBN: 978-81-965621-6-8

In this paper the excavation case history on Taipei National Enterprise Centre (TNEC) is adopted for the numerical analysis using the HSS soil model. The study results demonstrate that the Hardening-Soil with Small Strain stiffness (HSS) model is capable for predicting both the wall deflections and the surface settlements simultaneously.

2 Case Studied

The Taipei National Enterprise Center (TNEC), depicted in Figure 1, is a well-documented excavation case history presented by C. Y. Ou *et al.* (2000); C.-Y. Ou *et al.* (1998), Kung & Ou (2006), Kung *et al.* (2009) and C. Y. Ou (2016). The main observation section on the southeast of the excavation pit comprised an inclinometer in wall and 4 inclinometers in ground. The array of the settlement markers deployed next to the inclinometers SI1 to SI4 comprised 21 markers spacing at 1 m to 3 m. The array was extended to 49 m behind the south wall.

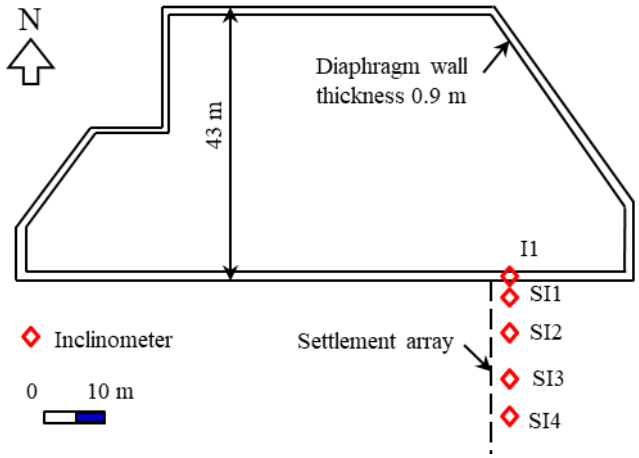

Figure 1: *Instrumentation layout of the Taipei National Enterprise Center (TNEC) excavation*

2.1 Ground conditions

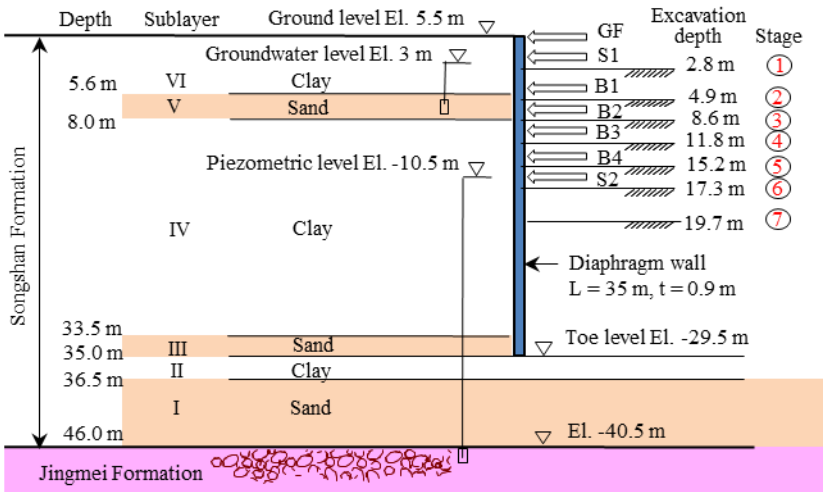

Figure 2: *Soil profile of the TNEC case and excavation scheme*

The TNEC building is located in the K1 Geological Zone (MAA 1987) in the eastern portion of the Taipei Basin. A representative excavation model is shown in Figure 2. The excavation was carried out to a depth of 19.7 m in 7 stages. The pit was retained by diaphragm wall of 0.9 in thickness and 35 m in length. Excavation for the foundation was constructed by the top-down method. The diaphragm wall was supported by the ground floor (GF) slab and 4 levels of basement floor slabs (B1 to B4) of 150 mm

Proceedings DOI: 10.21467/proceedings.159
ISBN: 978-81-965621-6-8

Series: AIJR Proceedings
ISSN: 2582-3922

in thickness. Temporary steel struts were erected at the upper and the lower levels (S1 & S2). Excavation commenced in January 1992 and the foundation slab at 19.7 m depth was cast in November 1992.

As depicted in the soil profile shown in Figure 2, the Songshan Formation of 46 m in thickness comprises six alternating sand (SM) and clay (CL) layers. Sublayers I, III, and V are sandy soils and Sublayers II, IV, and VI are clayey soils. The properties of the six sublayers in the Songshan Formation have been well discussed in literature (MOH & OU, 1979;-MAA 1987; Moh *et al.*, 1989). Underlying the Songshan Formation is a water-rich gravelly (GM) Jingmei Formation, which is a competent formation with very high stiffness.

2.2 Undrained shears strengths for clay sublayers

An advanced study was conducted by Geotechnical Engineering Specialty Consultant engaged by the Department of Rapid Transit Systems of Taipei City Government in the very early stage of the metro construction. This Designated Task studied the characteristics of the soils in the Taipei Basin to provide the basic information required for the design and construction of metro facilities (Chin *et al.* 1994 and 2007; Chin & Liu 1997; Hu *et al.* 1996). This was a research project so it was carried out under stringent supervision. Soil samples of high quality were obtained and tested with great care. The test results are therefore more reliable than those normally obtained. Figure 3 presents the results of the CK_0UC tests conducted on the specimens recovered from borehole R-1 that Chin *et al.* (1994) reported. Borehole R-1 was located in the K1 Geological Zone in Taipei Basin. Kung *et al.* (2009) and Ou *et al.* (2000a) presented the results of undrained shear strength, s_u, for the K1 Geological Zone in the Taipei Basin. The s_u values were determined from consolidated triaxial undrained compression and extension tests conducted on specimens recovered from the clayey Sublayer IV. The specimens were saturated and K_0-consolidated to the in-situ effective stress states. The undrained shear strengths to the vertical effective stresses, the s_u/σ'_v ratio, for the compression tests is 0.29. For the extension tests, the s_u/σ'_v ratio is 0.21. The variation in undrained shear strengths for the compression tests that Ou *et al.* (2000a) and Kung *et al.* (2009) reported are presented in Figure 3. Compared with the CK_0UC tests reported by Chin *et al.* (1994), the s_u values obtained by Ou *et al.* (2000a) and by Kung *et al.* (2009) are lower. The lower s_u values would likely be attributable to sampling disturbance. Although the specimens were consolidated to the in-situ horizontal stress, such process could not fully compensate the effect due to sample disturbance.

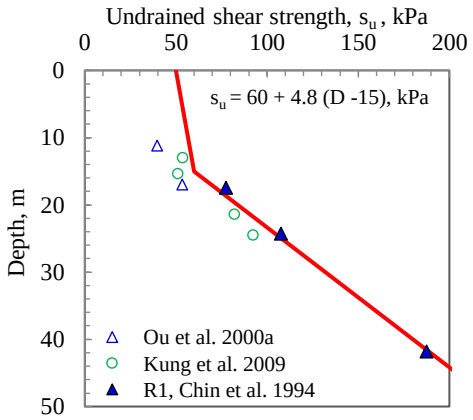

Figure 3: *Undrained shear strengths of clays obtained by CK_0UC triaxial tests.*

In this study, the Author has proposed the undrained shear strengths of the sublayers IV and II clayey soils in the K1 Geological Zone of the Songshan Formation could be expressed by the empirical equation:

$s_u = 60 + 4.8\ (D - 15)$ in kPa (1)

where D is the depth in metre and s_u is the undrained shear strength in kPa.

2.3 Groundwater conditions

The piezometric level in the Jingmei Formation was lowered to a level near the bottom of the Songshan Formation in the 1970s due to excessive extraction of groundwater to supply water to the city, leading to significant reductions in water pressures in the Songshan Formation and substantial ground settlements as a result. The piezometric level in the Jingmei Formation did not recover till 1974 although pumping had been banned since 1968. The subsoils in the Songshan Formation in the Taipei Basin are thus substantially over-consolidated. This is particularly true for the clayey Sublayer II because the underlying sandy Sublayer I is so permeable that the piezometric level in Sublayer I essentially dropped by the same magnitudes as those in the Jingmei Formation. Based on monitoring records at the deep well at Sun Yet Sin Memorial Hall, located at 1.2 km south of the TNEC project site, Hwang and Moh (2022) reported that the piezometric level in the Jingmei Formation in the eastern portion of the Taipei Basin was around El. -10.5 m in 1992. In the central portion of the Taipei Basin, the piezometric level in Jingmei Formation recovered to El. 0 m in 2017.

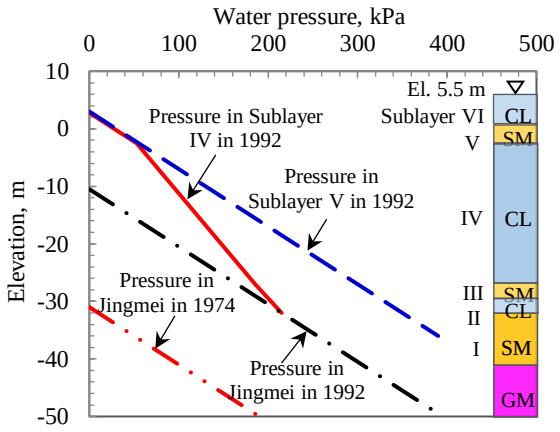

Figure 4: *Groundwater pressures on the outer face of the diaphragm walls*

C. Y. Ou *et al.* (2000) reported that the groundwater level in the Songshan Formation at TNEC was located at 2 m depth prior to excavation. The piezometric level of El. 3.0 m for the sublayers V is adopted for the numerical analysis in this study. The distributions of the water pressures outside the diaphragm wall at TNEC in 1992 are presented in Figure 4. For sublayer I and Jingmei Formation, the piezometric level of El. -10.5 m in 1992 is adopted. The water pressures for sublayers II to IV are interpolated between sublayers V and I. Inside the pit, the piezometric levels were maintained at a depth of 1 m below the excavation levels in each stage have been adopted in the analysis.

3 Numerical Simulation

3.1 Finite element mesh

The section for the numerical analysis is depicted in Figure 5. The width of the excavation is 40 m. Because of symmetry in geometry, only half of the section is analyzed as depicted in Figure 5. The excavation is carried out to a depth of 19.7 m in the analysis. The lateral extent of the finite element model reaches a distance of 140 m from the central axis of the excavation trench. The ground model is 60 m in depth and the diaphragm wall is located at a distance of 20 m from the axis of the trench.

Proceedings DOI: 10.21467/proceedings.159
ISBN: 978-81-965621-6-8

Series: AIJR Proceedings
ISSN: 2582-3922

The Jingmei Formation is a competent formation with very high stiffness and is frequently assumed to be the base of the numerical models. However, the base of the finite element model in this study is placed at a depth of 60 m to include a 14 m layer of the Jingmei Formation to ensure that the contribution of this formation to ground movements is accounted for.

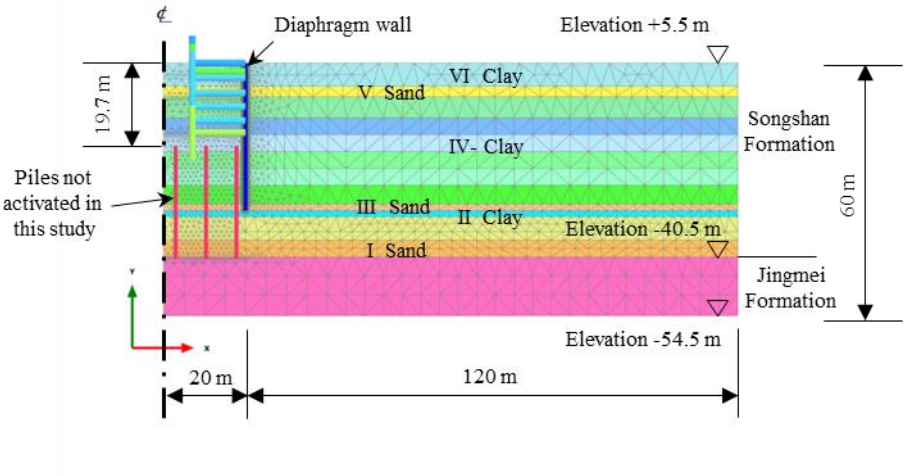

Figure 5: *Finite element mesh for the analytical section for 7 stages of excavation*

3.2 Nonlinearity of soil behavior - Hardening-soil with small-strain stiffness model

The PLAXIS-2D finite element software developed by PLAXIS BV (2013) has become a very popular tool in geotechnical analysis and design. The Hardening-Soil with Small-strain stiffness (HSS) constitutive soil model is an extension of the Hardening-Soil model (Benz Thomas 2006; Schanz *et al.* 1999; Schanz & Vermeer 1998) introduced in the PLAXIS program and is adopted herein to simulate the non-linear stress-strain relationship of soils under loading and unloading conditions. In the HSS model, the parameters adopted to define the hyperbolic stress-strain relationship are as follows:

- E^{ref}_{50} is the reference secant stiffness from standard triaxial drained test,
- E^{ref}_{oed} is the reference tangent stiffness for oedometer primary loading,
- E^{ref}_{ur} is the reference unloading-reloading stiffness from standard triaxial drained test,
- m is the exponential factor for stress-level dependency of stiffness,
- R_f is the failure ratio, $R_f = q_f / q_a$,
- q_a is the asymptotic value of the shear strength and q_f is the failure strength,
- G^{ref}_0 is the reference shear modulus at the level of very small strains,
- $\gamma_{0.7}$ is the reference shearing strain to define the behavior of degradation of moduli when G^{ref}_0 is reduced to 0.7 G^{ref}_0.

In this study, the stiffness values of soils are related to the undrained shear strengths for clays and the N values for sands as expressed in the empirical Equations 2 to 6:

$$E^{ref}_{50} = 150\ s_u \text{ (for clayey soils)} \quad (2)$$

$$E^{ref}_{50} = 2\ N \text{ (in MPa for sandy soils)} \quad (3)$$

$$E^{ref}_{oed} = E^{ref}_{50} \quad (4)$$

$$E^{ref}_{ur} = 5\ E^{ref}_{50} \quad (5)$$

$$G^{ref}_0 = E^{ref}_{ur} \quad (6)$$

in which s_u is the undrained shear strengths of clayey soils and N is the blow-counts obtained in standard penetration tests for sandy soils. The parameters adopted in this study are summarized in Table 1. The effective shear strength parameters, i.e., the c' and ϕ' values, for the silty sand strata, are determined from laboratory tests conducted on thin-wall tube specimens. For the clayey layers, c' = s_u and ϕ' = 0° is assumed in the analyses. The dilation angle, ψ', of 2°, 0°, and 3° are adopted for the sandy, the clayey, and the gravelly soils respectively. The R_f equals 0.9 is adopted. The unload-reload Poisson's ratio, υ_{ur}, of 0.2 is used as suggested by Benz Thomas (2006) and Schanz *et al.* (1999). Although the HSS soil model is an effective stress model and adopting the ϕ' = 0° for the clayey soils loses its compression hardening function and stress-dependent stiffness, parametric studies using both the effective and the total stress models show that the computed wall deflections and settlements are essentially the same. The total stress model for clay is adopted in this study.

Table 1: *Soil parameters for the HSS model adopted in the PLAXIS analyses.*

Mid depth m	Soil type	Unit weight γ' kN/m³	N value	Undrained shear strength s_u, kPa	Effective cohesion c' kPa	Effective friction angle ϕ', deg	Dilation angle ψ' deg	Reference stiffness, MPa		Initial shear moduli G^{ref}_0, MPa
								Secant stiffness E^{ref}_{50}	Unload-reload stiffness E^{ref}_{ur}, MPa	
2.8	CL	18.3	3	52				7.8	39	39
7	SM	18.9	5		0	31	2	10	50	50
11	CL	18.2	3	57				8.6	43	43
15.5	CL	18.2	4	62				9.4	47	47
19.5	CL	18.2	4	82				12.2	61	61
23.5	CL	18.2	7	101				15.1	76	76
27	CL	18.2	8	118				17.6	88	88
31	CL	18.2	5	137				20.5	103	103
34.5	SM	19.6	14		0	31	2	28	140	140
35	CL	19.1	10	163				24.5	122	122
39.3	SM	19.6	24		0	32	2	48	240	240
44	SM	19.6	20		0	32	2	40	200	200
53	GM	20.6	>100		0	35	3	300	1500	1500

3.3 Determination of small-strain stiffness

The parameters for the small-strain stiffness, i.e., the G^{ref}_0 and the $\gamma_{0.7}$, have been determined from the laboratory tests. Kung *et al.* (2009) presented the results of small-strain triaxial tests and bender element tests conducted on undisturbed specimens recovered from clayey Sublayer IV of the Songshan Formation. The specimens were saturated and K_0-consolidated to the in-situ effective stress states. The K_0 values applied for consolidation ranged from 0.5 to 0.55. After completing the K_0-consolidation, but prior to the shearing tests, bender element tests were carried out to measure the shear moduli of the clay specimens. Compression and extension undrained triaxial shearing tests were then conducted. The undrained shear strengths profile obtained is presented in Figure 3. Based on the results of the bender element tests, Kung *et al.* (2009) obtained the G_{max}/s_u ratios ranging from 738 to 788, with an average ratio of 759 for the axial compression tests, where G_{max} is the initial shear modulus. For the axial extension tests, the G_{max}/s_u ratios ranged from 614 to 751, with an average of 671. In this study, the G^{ref}_0 = 750 s_u is adopted.

Chin *et al.* (2007) presents the CK_0UDSS test results that are depicted in Figure 6. Santos & Correia (2001) recommended that the stress-strain curve for small-strains can be described as:

Proceedings DOI: 10.21467/proceedings.159
ISBN: 978-81-965621-6-8

Series: AIJR Proceedings
ISSN: 2582-3922

$$G / G_0 = 1 / (1+ 0.385\ \gamma / \gamma_{0.7}) \quad (7)$$

where G_0 is the maximum small-strain shear modulus. The modulus degradation curves with the threshold $\gamma_{0.7}$ values ranging from $0.8x10^{-4}$ to 10^{-3} are shown in Figure 7. The degradation of the shear moduli with shear strain interpreted from the direct simple shear test is presented Figure 7, showing that the Taipei clay would have the $\gamma_{0.7}$ value of 5 x 10^{-4}. In this study, a $\gamma_{0.7}$ value of 4 x 10^{-4} has been adopted.

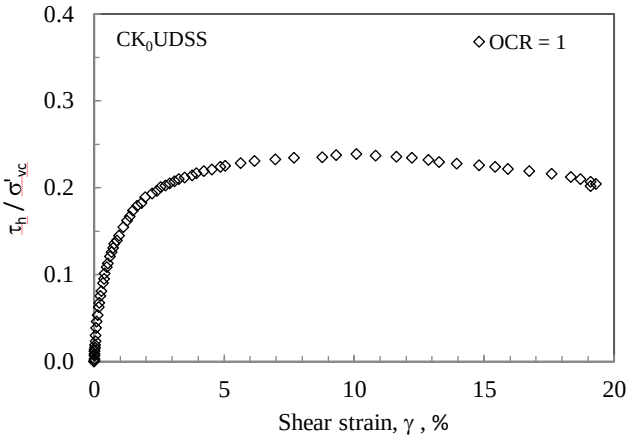

Figure 6: *Stress-strain curve of Taipei clay under CK0UDSS test (After Chin et al. (2007))*

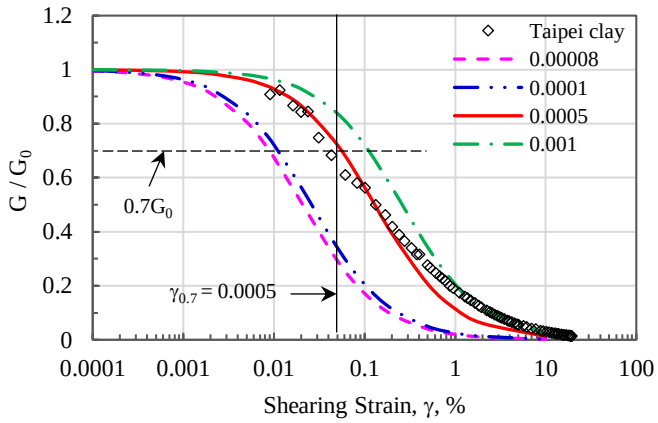

Figure 7: *Degradation of shear moduli with shearing strain*

3.4 Modeling of the retaining structures

The excavation scheme and the retaining structures are depicted in Figure 2. The diaphragm wall is simulated by plate element and an E_c value of 25,000 MPa is adopted for concrete with a characteristic compressive strength of 28 MPa. The estimated flexural rigidity (denoted as E_cI_c where I_c is the moment of inertia) and the axial stiffness (denoted as E_cA_c where A_c is the sectional area) of the diaphragm wall of 0.9 m in thickness are 1,067 MN-m and 15,810 MN/m respectively. These values have already been reduced from their original values by 30 % to account for tensile cracks and creeping of concrete during excavation.

The excavation was supported by 5 levels of floor slabs, namely, the ground level floor (GF) and the 4 basement floors (B1 to B4) of 150 mm in thickness and 2 levels of steel struts. During the top-down construction, openings were provided on the floor slabs for transportation of excavated materials and

for delivery of construction materials such as reinforcement bars, concrete and the steel struts. In addition to the concrete creeping effect, the axial stiffnesses of the floor slabs have been further reduced by 30 % for the openings. For the combining effect of creeping and the presence of opening, a reduction factor of 0.5 is adopted. The axial stiffness of 1,988 MN/m is adopted for the slabs GF and B1 to B4 in the numerical analysis. The level S1 struts were erected at the depths of 2 m prior to the construction of the GF slab.

Table 2: *Strut properties*

Strut level	Depth m	Strut type	Area A_s, cm^2	Stiffness E_sA_s/s, MN/m	Design preload, kN/m	Strut spacing s, m
S1	2.0	1H300x300x10x15	118.5	714	231	3.4
S2	16.5	1H400x400x13x21	218.7	1,319	346	

The slabs and the struts are represented by fixed-end anchors. The properties for the steel struts are presented in Table 2. The steel is assumed to be an elastic material with a Young's modulus (E_s) of 210 GPa.

3.5 Modeling of soil-structure interface

The contact between the soil and the wall structure is a critical issue to be considered in deep excavations. A frictional contact model is applied at the soil-wall interface to investigate its influence on the wall deflection and on the surface settlement behavior. In the PLAXIS software, an elastic-plastic model following the Mohr-Coulomb criterion is used to describe the interfaces for the soil-structure interaction. According to the Reference Manual (Bentley, 2022), the strength properties of the interface are related to the strength properties of a soil layer by a strength reduction factor, $R_{inter,}$ and are calculated by applying the following rules:

$$s_{u,i} = R_{inter}\, s_{u,\,soil} \quad (8)$$

$$\tan \phi_i = R_{inter} \tan \phi_{soil} \quad (9)$$

$$\psi_i = 0 \text{ for } R_{inter} < 1, \text{ otherwise } \psi_i = \psi_{soil} \quad (10)$$

where $s_{u,\,i}$, ϕ_i , ψ_i are the undrained shear strength, the friction angle and the dilation angle of the interface. It is noted that the interface stiffness is also linked to the R_{inter} value by the expressions:

$$G_i = R^2_{inter}\, G_{soil} \quad (11)$$

$$E_{oed,i} = 2\, G_i\, (1 - \nu_i) / (1 - 2\, \nu_i) \quad (12)$$

where the G_i is the shear moduli and the $E_{oed,i}$ is the compression moduli of the interface. The Poisson's ratio of the interface, ν_i , is 0.45. The R_{inter} value of 1 is the rigid mode and represents the rough interface. In this study, various R_{inter} values have been adopted to assess the influence of soil-structure interaction. As summarized in Table 3, Case 1, Case 2 and Case 3 adopt the R_{inter} values of 1, 0.5 and 0.3 respectively.

Proceedings DOI: 10.21467/proceedings.159
ISBN: 978-81-965621-6-8

Series: AIJR Proceedings
ISSN: 2582-3922

4 Results Of Numerical Analysis

4.1 Computed wall deflections

The computed wall deflection profiles for the TNEC case are presented in Figure 8. The analysis results are compared with those observed at inclinometers I-1 that C. Y. Ou *et al.* (2000) reported. Close matching of the computed profiles with those observed has been achieved for Case 3 adopting the R_{inter} = 0.3. In the final stage the computed maximum deflection, $\delta_{h\text{-}max}$, is 109.7 mm, which deviates from the observed 106.4 mm by only 3 %. The computed wall deflections and surface settlements for Case 1 to Case 3 are summarized in Table 3, showing a trend that the smaller R_{inter} value, the larger wall deflections would be computed. The $\delta_{h\text{-}max}$ values of 109.7mm and 98.7 mm are computed for the cases adopting the R_{inter} values of 0.3 and 1 respectively. Smooth interfaces (R_{inter} < 1) would give larger wall deflections than those for the rough interface.

Table 3: *Computed wall deflections and surface settlements in the final stage*

Case	Interface reduction R_{inter}	Wall deflection, mm		Wall settlement, mm			Surface settlement, mm		Settlement between wall & ground, mm
		Maximum $\delta_{h\text{-}max}$	At toe $\delta_{h\text{-}toe}$	At top	At toe	Short-ening	Maximum $\delta_{v\text{-}max}$	Next to wall	
Observed	-	106.4	11.4	-	-	-	74	40	-
1	1	98.7	7.4	5.0	4.4	0.6	57.0	4.1	-0.9
2	0.5	93.6	9.0	8.0	7.5	0.5	63.0	13.2	5.2
3	0.3	109.7	14.2	18.4	18.1	0.3	77.3	30.0	11.6

4.2 Computed lateral ground movements

Along the instrumented section at the southeast area of the excavation pit, the inclinometers in ground SI-1 to SI-4 were installed at the distances of 2 m to 22 m behind the diaphragm wall. C. Y. Ou *et al.* (2000) and Kung *et al.* (2009) reported the ground movement profiles observed at these inclinometers. Figure 9 presents the computed ground movements in the final stage for Case 3 adopting the R_{inter} value of 0.3. The computed lateral ground movement profiles closely match with those observed at SI-1 to SI-4.

It is noted that inclinometers SI-3 and SI-4 were 30 m in length and were not embedded into the Jingmei Formation. The numerical analysis shows that the toe movements of 19 mm and 12 mm would occur at the toe levels of these inclinometers in the final stage. The lateral deflection profiles for SI-3 and SI-4 shown in Figure 9 are therefore adjusted by adding the computed toe movement values.

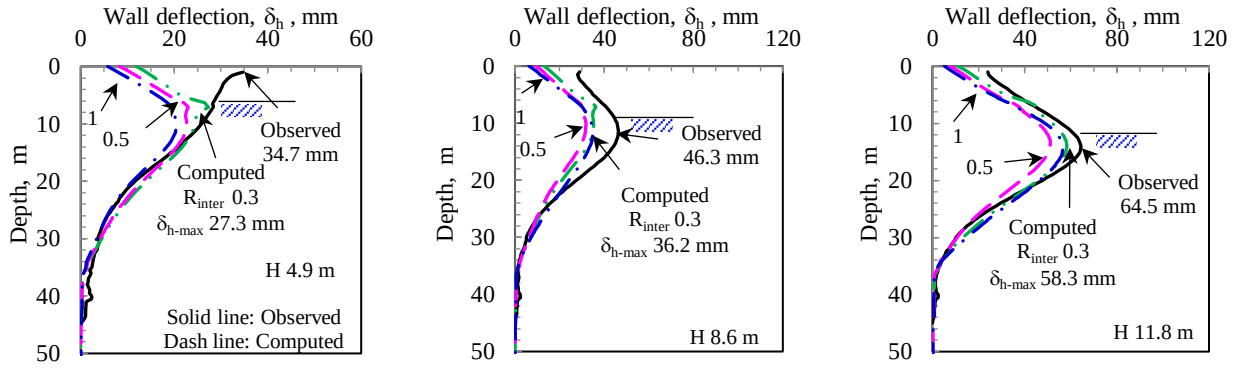

(a) Stage 2 (b) Stage 3 (c) Stage 4

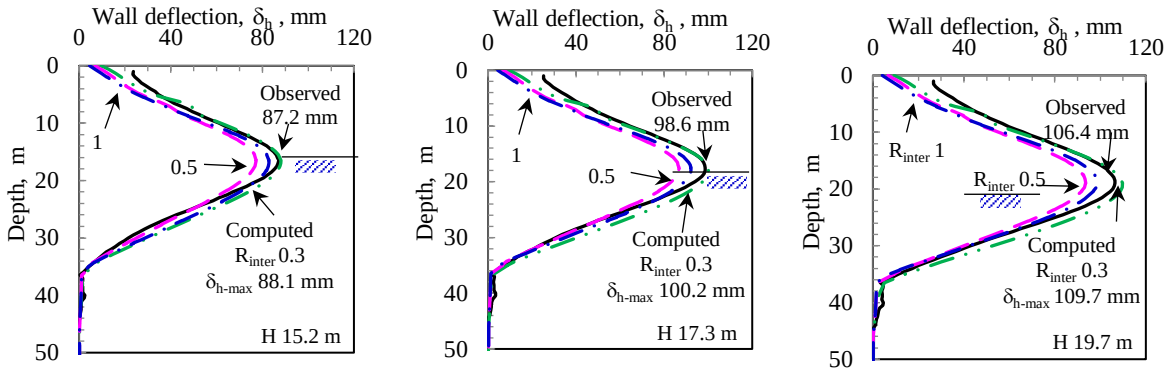

(d)Stage 5 (e) Stage 6 (f) Stage 7

Figure 8: *Computed and observed wall deflections for Stage 2 to Stage 7 – Case 1 to Case 3*

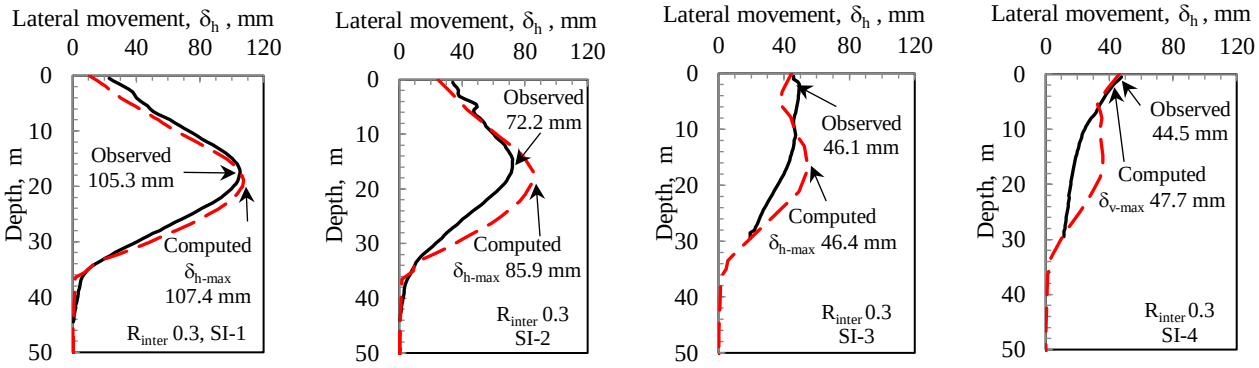

(a) 2m behind wall (b) 8 m behind wall (c) 16 m behind wall (d) 22 m behind wall

Figure 9: *Computed and observed lateral ground movements in final stage at various distances behind wall - Case 3*

4.3 Computed surface settlements

Figure 10 presents the computed surface settlements for Case 1 to Case 3 in Stage 2 to Stage 7. Compared with the observed settlements that Kung & Ou (2006) reported, close matching between the analyzed and the observed has been achieved in the final Stage for Case 3, which adopts the R_{inter} value of 0.3. In the final Stage the computed maximum settlement, $\delta_{v\text{-}max}$, is 77.3 mm, which over-estimates the observed 74 mm by 4.5 %. Compared with the surface settlements predicted by other nonlinear soil models that Kung & Ou (2006) presented, the results obtained in this study by the HSS model is considered as satisfactory.

Table 3 shows that the computed $\delta_{v\text{-}max}$ in the final stage for Case 1 adopting the R_{inter} value of 1 is 57.0 mm, which deviates from the observed $\delta_{v\text{-}max}$ of 74 mm by 23 %. For Case 2 adopting the R_{inter} value of 0.5, the computed $\delta_{v\text{-}max}$ of 63.0 mm deviates from the observed 74 mm by 15 %. As summarized in Table 3, there is a trend that the smaller the R_{inter} value, or the smoother along the soil-wall interface, the larger surface settlements would occur.

Proceedings DOI: 10.21467/proceedings.159
ISBN: 978-81-965621-6-8

Series: AIJR Proceedings
ISSN: 2582-3922

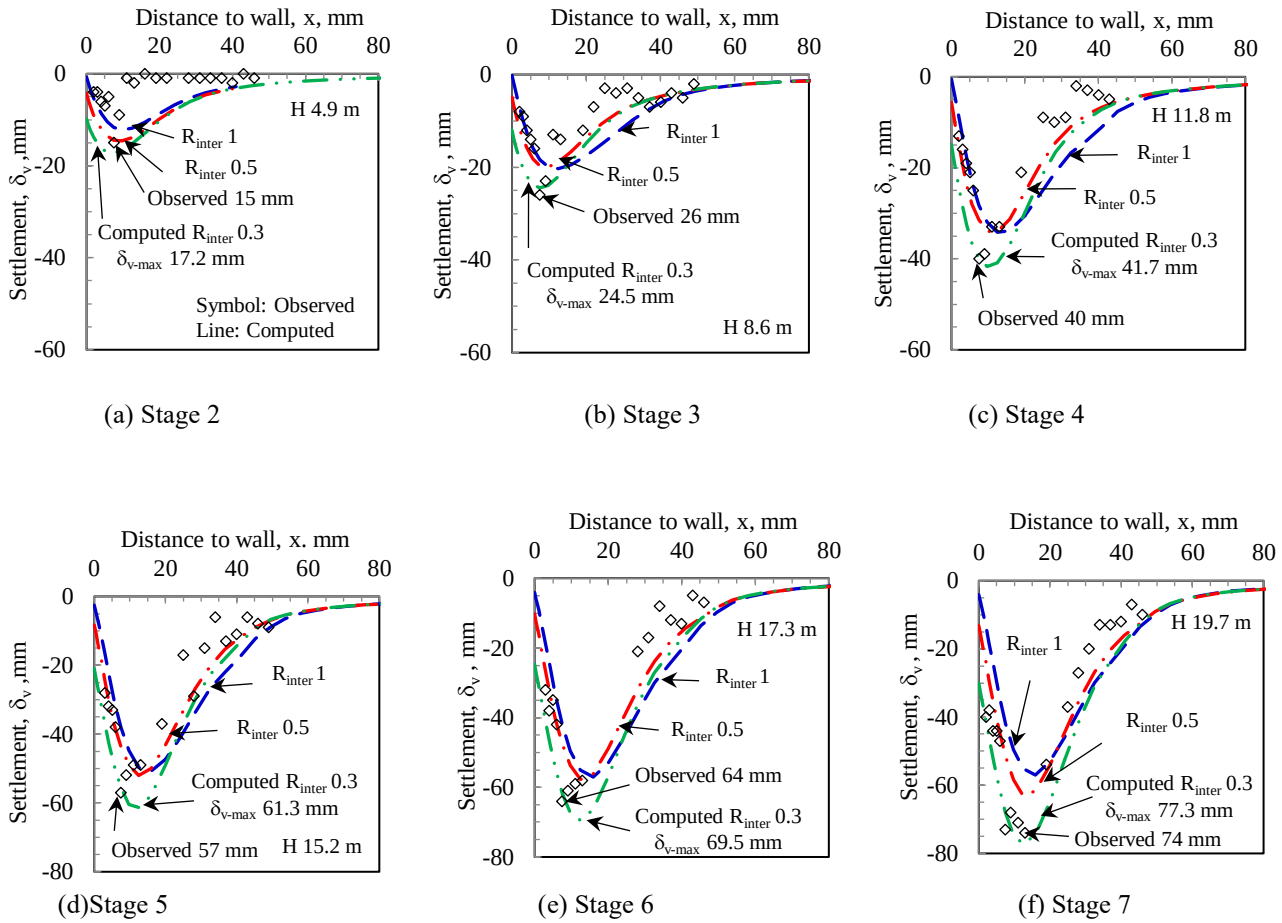

Figure 10: *Computed and observed surface settlements in Stage 2 to Stage 7 – Case 1 to Case 3*

4.4 Normalized settlement profiles

Figure 11 presents the normalized computed and observed settlement profiles in the final Stage for Case 1 to Case 3. The surface settlements, δ_v, are normalized with the maximum settlement, $\delta_{v\text{-}max}$. The distances to the wall, the x values, are normalized with the excavation depth, H. While close matching between the computed and the observed normalized profiles is achieved at the distance within 1H behind the wall, the computed results for these 3 cases would over-estimate the settlements at the distances between 1H and 2.5H. Case 3 would slightly over-estimate the surface settlements by $0.13\delta_{v\text{-}max}$ at the distance of 1.6H to the wall. For Case 2 and Case 1, the over-estimation would increase to $0.18\delta_{v\text{-}max}$ and $0.25\delta_{v\text{-}max}$ respectively at that distance.

Case 3 has the narrowest width of the settlement trough. Measuring at $0.2\delta_{v\text{-}max}$, the width of the normalized settlement trough is approximately 2.1H for Case 3. For Case 2 and Case 1, the widths of the troughs are approximately 2.3H and 2.4H respectively. Amongst these 3 cases, the shape of the settlement trough for Case 3 has the closest matching with that observed.

Figure 11 shows that at the distance immediately next to the wall at x = 0, the computed normalized settlements, $\delta_v/\delta_{v\text{-max}}$, for the cases adopting the R_{inter} values of 1, 0.5 and 0.3 are 0.07, 0.21 and 0.39 respectively. The numerical analysis in this study shows that the lower the R_{inter} value, the larger settlements would occur next to the wall. The interface reduction factor, R_{inter}, would be the key parameter for assessing the surface settlements behind the retaining structures.

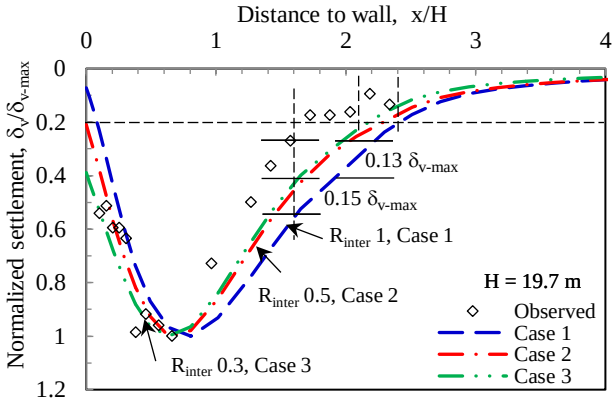

Figure 11: *Normalized computed and observed surface settlements in final stage - Case 1 to Case 3*

4.5 Settlements of the wall

The effect of soil-structure interface to wall and ground movements can be seen from the results of parametric studies presented in Table 3. There is the trend that the lower the R_{inter} values, the less shortening of the wall. Deducing from the wall top and the wall toe settlements, the wall shortening would be 0.6 mm with the rough interface ($R_{inter} = 1$). With the smooth interfaces, R_{inter} of 0.5 and 0.3, the wall shortening would be 0.5 mm and 0.4 mm respectively. This implies that the soil frictions acting along the wall would be largest for the rough interface and the soil frictions would be less for the smooth interfaces ($R_{inter} < 1$).

The relative settlements between the wall and the soil immediately behind can be deduced from the wall top settlements and the surface settlements next to the wall. With the rough interface R_{inter} of 1, the relative settlement between the wall and the ground would be 0.9 mm. With the smooth interface R_{inter} of 0.3, the relative settlement would be as large as 11.6 mm. The smooth interface would give the apparent “slippage” along the soil-wall interface.

4.6 Effect of water pressures

In addition to the groundwater pressures in 1992 that Case 3 adopted, the performance of excavation with the piezometric levels in Jingmei Formation in 2023 and in 1974 have been studied. The piezometric levels of El. 0 and El. -31 in Jingmei Formation for Case 4 and Case 5 respectively are analyzed. Table 4 summarized the piezometric levels adopted for Case 3 to Case 5. The R_{inter} value of 0.3 is adopted for these cases.

Proceedings DOI: 10.21467/proceedings.159
ISBN: 978-81-965621-6-8

Series: AIJR Proceedings
ISSN: 2582-3922

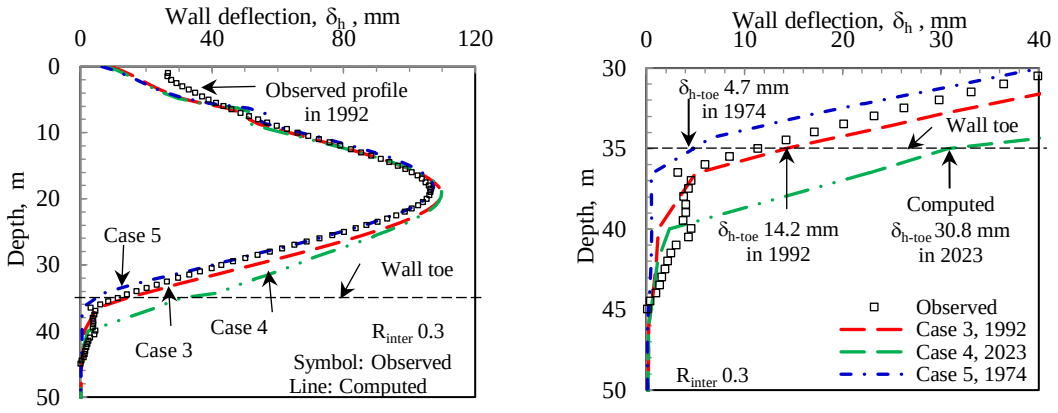

(a)Deflection profiles (b)Computed toe deflections

Figure 12: *Wall deflections in the final stage with various piezometric levels in Jingmei Formation - Case 3 to Case 5*

Table 4: *Computed wall deflections for various piezometric levels in Jingmei Formation*

Case	Piezometric level in Jingmei Formation, El. m	Year	Wall deflection, mm		Difference in deflection, mm	
			Maximum	At toe	Maximum	At toe
Observed	-10.5	1992	106.4	11.4	-	-
3	-10.5	1992	109.7	14.2	3.3	2.8
4	0	2023	109.8	30.8	3.4	19.4
5	-31.0	1974	107.3	4.7	0.9	-6.7

The computed wall deflections in the final stage for Case 3 to Case 5 are presented in Figure 12 and summarized in Table 4. The computed maximum wall deflections for Case 3 and Case 4 are within 3.4 mm of those observed. The groundwater pressure effect would be minimal to the maximum wall deflections.

The wall toe deflections are however sensitive to the groundwater pressures. Table 4 shows that the computed toe deflection, $\delta_{h\text{-}toe}$, would be as large as 30.8 mm for Case 4, which adopts the piezometric level in the Jingmei Formation at El. 0 m in 2023. Compared with the toe deflection of 11.4 mm observed in 1992, the computed $\delta_{h\text{-}toe}$ value for Case 4 would be 2.7 times of that occurred in 1992. For the scenario that the excavation would be conducted in 1974 with the piezometric level in the Jingmei Formation as low as El. -31 m in Case 5, the computed $\delta_{h\text{-}toe}$ is 4.7 mm, which would be 40 % of that occurred in 1992.

The effect of water pressures plays an important role on the performance of the deflections at the wall toe levels. The toe deflections as large as 30 mm would be crucial for interpreting the wall deflection profiles from inclinometers not embedded in competent stratum.

5 Conclusions

Two-dimensional numerical analysis on an excavation case history in soft ground has been conducted. The maximum excavation depth of 19.7 m was supported with diaphragm wall of 0.9 m in thickness and by top-down construction. The nonlinear Hardening-soil with small-strain stiffness (HSS) soil model is adopted. The following conclusions could be drawn:

(1) The nonlinear HSS soil model could reliably estimate the wall deflections, lateral ground movements behind the wall and the surface settlements simultaneously.

(2) The parametric study adopting various interface reduction factors shows that the performance of surface settlements behind the wall is intimately affected by the shear strengths developed along the soil-structure interface. The lower in the interface reduction factor, the larger wall deflections, wall settlements and surface settlements would be computed.

(3) The smooth interface would give the apparent "slippage" along the soil-wall interface. Such slippage would occur at the interface reduction factor around 0.3.

(4) The water pressure in the underlying water bearing strata is a key factor for assessing the wall performance especially at the toe level.

The set of stiffness parameters obtained from the small-strain triaxial tests and bender element tests have been verified by the TNEC excavation case history and could be the reference for studying other cases in the K1 Geological Zone of the Taipei Basin. The interface reduction factor would be the key parameter for exploring the ground movements due to deep excavations.

6 Publisher's Note

AIJR remains neutral with regard to jurisdictional claims in institutional affiliations.

How to Cite

L.W. Wong (2023). Effects of Soil-Structure Interaction on Wall Deflections and Surface Settlements During Deep Excavations. *AIJR Proceedings*, 63-77. https://doi.org/10.21467/proceedings.159.7

References

Bentley. (2022). PLAXIS 2D-Reference Manual. In *Bentley Advancing Infrastructure* (Connect V22.01). Bentley Advancing Infrastructure. https://communities.bentley.com/cfs-file/__key/communityserver-wikis-components-files/00-00-00-05-58/PLAXIS_5F00_3D_5F00_CEV22.01_5F00_0_2D00_Gen_2D00_Info.pdf

Benz Thomas. (2006). *Small-Strain Stiffness of Soils and its Numerical Consequences* [Institute of Geotechnics]. https://www.igs.uni-stuttgart.de/dokumente/Mitteilungen/55_Benz.pdf

Burland, J. B. (1989). Ninth Laurits Bjerrum Memorial Lecture: "Small is beautiful"—the stiffness of soils at small strains. *Canadian Geotechnical Journal*, *26*(4), 499–516. https://doi.org/10.1139/T89-064

Chin, C.T., Chen, J.R., Hu, I.C., Yao, D.H.C. & Chao, H.C. (2007), Engineering characteristics of Taipei clay. In T.S. Tan, K.K. Phoon, D.W. Hight & S. Leroueil (Eds), entitled: Characterization and Engineering Properties of Natural Soils, Taylor & Francis Group, v3:1755-1803.

Chin, C.T., Crooks, A.J.H. & Moh, Z.C. (1994). Geotechnical properties of the cohesive Sungshan deposits. Geotechnical Engineering, J. Southeast Asian Geotechnical Society, Taipei, Taiwan 25(2): 77-103. (in Chinese)

http://seags.ait.asia/e-journal/1970-2012/GEJ_1994_v25n2_December.pdf

Chin, C.T. & Liu, C-C. (1997). Volumetric and undrained behaviors of Taipei silty clay. J. Chinese Institute of Civil and Hydraulic Engineering, Taipei, Taiwan 9(4): 665-678. (in Chinese)

Duncan, J. M., & Chang, C.-Y. (1970). Nonlinear Analysis of Stress and Strain in Soils. *Journal of the Soil Mechanics and Foundations Division*, *96*(5), 637–659. https://doi.org/10.1061/JSFEAQ.0001458

Hu. I.C., Chin, C.T. & Liu, C.J. (1996). Review of the geotechnical characteristics of the soil deposits in Taipei, Sino-Geotechnics, No. 54: 5-14. (in Chinese)

Hwang, R. & Moh, Z.C. (2022). Groundwater drawdown and subsidence in the Taipei Basin. Sino-Geotechnics, No. 173/2022.9: 99-110. (in Chinese) http://www.geotech.org.tw/purchase-inner.php?id=202

Jardine, R.J., Potts, D.M., Fourie, A.B. & Burland J.B. (1986). Studies on the influence of non-linear stress-strain characteristics in soil-structure interaction. Geotechnique, Vol. 36, No. 2: 377-396.

Kondner, R.L. & Zelasko, J.S. (1963). A hyperbolic stress-strain formulation of sands. Proceedings of the 2nd Pan American Conference on Soil Mechanics and Foundation Engineering. San Paulo, Brazil, 1963. Associacao Brasileira de Mecanica dos Solos, Vol 1: pp 289–324

Kung, G. T. C., Ou, C. Y., & Juang, C. H. (2009). Modeling small-strain behavior of Taipei clays for finite element analysis of braced excavations. *Computers and Geotechnics*, *36*(1–2), 304–319. https://doi.org/10.1016/J.COMPGEO.2008.01.007

Kung, T.C. (2003). Surface settlement induced by excavation with consideration of small-strain behavior of Taipei silty clay. Ph.D. Dissertation, National Taiwan University of Science and Technology, Taiwan.

Kung, T.C. & Ou, C.Y. (2006). Prediction of surface settlement caused by excavation. Taylor & Francis Group plc, London UK: 853-858.

MAA (1987) Engineering properties of the soil deposits in the Taipei Basin, Report No. 85043, Ret-Ser Engineering Agency and Taipei Public Works Department, Taipei. (in Chinese)

Moh, Z. C., Chin, C. T., Liu, C. J., & Woo, S. M. (1989). Engineering correlations for soil deposits in taipei. *Journal of the Chinese Institute of Engineers* , *12*(3), 273–283. https://doi.org/10.1080/02533839.1989.9677162

MOH, Z. C., & OU, C. D. (1979). Engineering characteristics of Taipei Silt. *Proceedings of the Sixth Asian Regional Conference on Soil Mechanics and Foundation Engineering*, 155–158. http://seags.ait.asia/publications/6th-ARC-1979-Singapore-v1.pdf

Ou, C. Y. (2016). Finite Element Analysis of Deep Excavation Problems. *Journal of Geo Engineering*, *11*(1), 1–12. https://doi.org/10.6310/JOG.2016.11(1).1

Ou, C. Y., Shiau, B. Y., & Wang, I. W. (2000). Three-dimensional deformation behavior of the Taipei National Enterprise Center (TNEC) excavation case history. *Canadian Geotechnical Journal*, *37*(2), 438–448. https://doi.org/10.1139/T00-018

Ou, C.Y., Liao, J.T. & Cheng, W.L. (2000a), Building response and ground movements induced by a deep excavation, Geotechnique, Vol. 50, No. 3: 209-220.

Ou, C.-Y., Liao, J.-T., & Lin, H.-D. (1998). Performance of Diaphragm Wall Constructed Using Top-Down Method. *Journal of Geotechnical and Geoenvironmental Engineering*, *124*(9), 798–808. https://doi.org/10.1061/(ASCE)1090-0241(1998)124:9(798)

PLAXIS B.V. (2013). PLAXIS Reference Manual. PLAXIS, BV, Delft, the Netherlands.

Roscoe, K. H., & .Burland, J. B. (1968). On the generalized stress-strain behavior of “wet” clay: 60. K. H. Roscoe and J. B. Burland. Engineering Plasticity (Papers for a conference held in Cambridge, Mar. 1968), Cambridge, University Press, 535–609 (1968). *Journal of Terramechanics*, *7*(2), 107–108. https://doi.org/10.1016/0022-4898(70)90160-6

Santos, J. A. Dos, & Correia, A. G. (2001). Reference threshold shear strain of soil. Its application to obtain an unique strain-dependent shear modulus curve for soil. *In 15th Int. Conf. SMGE*. https://www.issmge.org/publications/online-library

Schanz, T. & Vermeer, P.A. (1998). On the Stiffness of Sands. Geotechnique, 46, No. 1: 145-151.

Schanz, T., Vermeer, P. A., & Bonnier, P. G. (1999). The hardening soil model: formulation and verification. In *Beyond 2000 in Computational Geotechnics* (pp. 281–290). Routledge. https://communities.bentley.com/cfs-file/__key/communityserver-wikis-components-files/00-00-00-01-05/The_5F00_Hardening_5F00_Soil_5F00_Model_5F002D005F00_Formulation_5F00_and_5F00_Verfication.pdf

STALLEBRASS, S. E., & TAYLOR, R. N. (1997). The development and evaluation of a constitutive model for the prediction of ground movements in over consolidated clay. *Geotechnique*, *47*(2), 235–253.